PCP
PLANT & CELL PHYSIOLOGY

Functional Water Flow Pathways and Hydraulic Regulation in the Xylem Network of Arabidopsis

Joonghyuk Park[1,4], Hae Koo Kim[2,3,4,5], Jeongeun Ryu[2,3], Sungsook Ahn[2,3], Sang Joon Lee[2,3,*] and Ildoo Hwang[1,*]

[1]Department of Life Sciences, Pohang University of Science and Technology, Pohang 790-784, Korea
[2]Center for Biofluid and Biomimic Research, Pohang University of Science and Technology, Pohang 790-784, Korea
[3]Department of Mechanical Engineering, Pohang University of Science and Technology, Pohang 790-784, Korea
[4]These authors contributed equally to this work.
[5]Present address: Global Conservation Agriculture Program, International Maize and Wheat Improvement Center (CIMMYT), P.O. Box 5689, Addis Ababa, Ethiopia.
*Corresponding authors: Sang Joon Lee, E-mail, sjlee@postech.ac.kr; Fax, +82-54-279-3199; Ildoo Hwang, E-mail, ihwang@postech.ac.kr; Fax, +82-54-279-0629.
(Received October 7, 2014; Accepted December 5, 2014)

Regular Paper

In vascular plants, the xylem network constitutes a complex microfluidic system. The relationship between vascular network architecture and functional hydraulic regulation during actual water flow remains unexplored. Here, we developed a method to visualize individual xylem vessels of the 3D xylem network of *Arabidopsis thaliana*, and to analyze the functional activities of these vessels using synchrotron X-ray computed tomography with hydrophilic gold nanoparticles as flow tracers. We show how the organization of the xylem network changes dynamically throughout the plant, and reveal how the elementary units of this transport system are organized to ensure both long-distance axial water transport and local lateral water transport. Xylem vessels form distinct clusters that operate as functional units, and the activity of these units, which determines water flow pathways, is modulated not only by varying the number and size of xylem vessels, but also by altering their interconnectivity and spatial arrangement. Based on these findings, we propose a regulatory model of water transport that ensures hydraulic efficiency and safety.

Keywords: *Arabidopsis thaliana* • Gold nanoparticle • Hydraulic regulation • Synchrotron X-ray CT • Water transport • Xylem network.

Abbreviations: AuNP, gold nanoparticle; DAB, days after bolting; SEM, scanning electron microscopy; SXRCT, synchrotron X-ray computed tomography; VB, vascular bundle.

Introduction

Water uptake and transport in vascular plants are topics of great interest to plant scientists (Dixon and Joly 1894, Johnson and Dixon 1965, Tyree 1997, Wei et al. 1999, Zwieniecki et al. 2001, Tyree and Zimmermann 2002, Wheeler and Stroock 2008). Vascular plants contain a complex and redundant xylem vessel network that transports water through the plant using the tensile forces created mainly by transpiration. The basic components of the xylem are similar in ferns, conifers, monocots and dicots: conduits (tracheids or vessel) form water-conducting tubes that, together with fiber cells, provide mechanical support for the plant body (Tyree and Zimmermann 2002).

Water transport through the xylem is finely regulated by environmental conditions and the water demand of the different organs of the plant. Conventionally, to examine xylem sap transport and functional water flow pathways, an aqueous dye such as fuchsin or safranin was injected into xylem vessels and the dyed vessels were traced at the height above the dye injection as the water-conducting pathway (Harris 1961, Sano et al. 2005, Umebayashi et al. 2007). As a non-destructive imaging method, nuclear magnetic resonance (NMR) can be employed to visualize xylem in intact samples with a spatial resolution of around 20 μm (Wistuba et al. 2000, Holbrook et al. 2001, Scheenen et al. 2007, Van As 2007). However, because the relatively low spatial resolution of these methods precludes visualization of water flow in individual xylem vessels (Kim et al. 2014), a more realistic view of the hydraulic map that takes the spatial arrangement of individual vessels in the xylem network into account (Holbrook and Zwieniecki 2005) is essential for understanding water transport. Recently, high-resolution synchrotron X-ray imaging was used to visualize xylem structure non-destructively with a spatial resolution typically around 1 μm (Brodersen et al. 2010, Kim and Lee 2010, Brodersen et al. 2012). In particular, synchrotron X-ray computed tomography (SXRCT) enables evaluation of both the structure and function of the plant xylem network in three dimensions in a relatively short time. It is advantageous to study samples using virtual serial sections in any plane that is physically difficult in using traditional microscopic methods. The interconnectivity of the 3D xylem network needs to be emphasized to understand the regulation of water-conducting activities (Loepfe et al. 2007). The ionic composition of sap also affects xylem sap flow by changing pit membrane permeability and sap fluidity (Zwieniecki et al. 2003, Lee et al. 2012, Santiago et al. 2013, Ryu et al. 2014).

Plant Cell Physiol. 56(3): 520–531 (2015) doi:10.1093/pcp/pcu198, Advance Access publication on 16 December 2014, available online at www.pcp.oxfordjournals.org

Here, we developed reliable methods in which gold nanoparticles (AuNPs) are used as flow tracers in SXRCT to investigate the water-conducting activities of individual xylem vessels during water transport through the 3D xylem network of the model plant *Arabidopsis thaliana*, which is suitable for visualization of a whole stem with high resolution due to its small diameter. Scanning electron microscopy (SEM) coupled with AuNPs is used to observe the direction of lateral flow via intervessel pits. Based on our analyses, we propose a model of water transport that incorporates newly classified vascular bundle (VB) types and the effect of compartmentalization of xylem vessels into clusters within a VB.

Results

Tracking water flow in individual xylem vessels using AuNPs coupled with SXRCT and SEM analysis

To generate a hydraulic map of the xylem network in Arabidopsis with the small xylem vessels (diameter of 5–30 μm), we measured the water-conducting activities of individual xylem vessels by using SXRCT combined with AuNPs at a given point (i.e. at a specific height of the stem) with cut stems. The cut stem was used because AuNPs cannot be introduced into intact plants via roots. However, because air bubbles could be generated by severing the stem even under water (Wheeler et al. 2013), we confirmed that the stem sections cut under water and immediately frozen in liquid nitrogen have no embolized vessels, whereas some embolized vessels were observed in the sections cut in air (**Supplementary Fig. S1**). AuNPs were introduced into the cut ends of the stems and used as tracers to ensure that the value obtained is specific to a single vessel in the network. In contrast to general hydrophilic dyes used to visualize water flow, AuNPs do not pass through non-porous pit membranes in Arabidopsis (Tixier et al. 2013). Thus, AuNPs in AuNP solution accumulated in the xylem vessel lumen near the base of the cut stems (**Supplementary Fig. S2**). As shown in **Fig. 1A**, SXRCT clearly detected AuNP accumulation in each xylem vessel within a stem, and the strength of the signal reflected the amount of accumulated AuNPs and allowed the water-conducting activity of individual xylem vessels to be estimated. However, considering that AuNP accumulation might block sap flow through pits after an extended period of uptake of AuNP solution, we validated and optimized the experimental conditions. First, to select appropriate samples, we measured the water uptake volume of intact plants from which soil had been removed (**Supplementary Fig. S3A**). Water uptake is saturated in plants (stem length >30 cm) over 17 days after bolting (DAB), indicating that plants at this stage are sufficiently developed for water flow analysis. Secondly, to ensure the integrity of cut stems in water transport, we compared the volume of water uptake by cut stems and by plants from which the rosette leaves had been removed. Stems cut under water to prevent embolisms from forming and plants from which the rosette leaves had been removed were transferred to water-containing vials, and the volume remaining in the vials was measured at 10-min intervals for 1 h. The water uptake volume of the two groups was very similar (**Supplementary Fig. S3B**), showing that the cut stems are indeed able to conduct water. Thirdly, we compared the volume of water and AuNP solution taken up by cut stems, and found that the volumes were almost identical during the first 30 min (**Fig. 1B**). However, after this time point, the uptake volume of AuNP solution lagged slightly behind that of water, indicating that extended uptake of AuNP solution had a small effect on sap flow. Therefore, we performed all AuNP uptake experiments within 30 min of exposure to the solution. Finally, the volume of AuNP solution taken up by the cut stems was closely correlated with the amount of AuNPs accumulated in xylem vessels within 30 min of exposure (**Fig. 1C**). The difference in absolute values between the volume of accumulated AuNPs and the volume of AuNP solution uptake was due to the low concentration of AuNPs in the solution (Ahn et al. 2010). Furthermore, the intervessel pits were not blocked with AuNP within 30 min (**Fig. 1D, E**). AuNPs could accumulate on pits after a long period of incubation (>1 h), which enables us to trace lateral water flow among conducting xylem vessels and surrounding tissues (**Fig. 1F, G**). SEM imaging after 1 h of AuNP solution uptake revealed that AuNPs were specifically deposited at one side of the intervessel pits, which indicated the direction of lateral flow between adjacent xylem vessels. Also, we found that the direction of lateral water flow depended on the xylem vessel position within a VB. In metaxylem vessels located near the pith and protoxylem, lateral water flow was oriented toward the protoxylem, whereas the metaxylem vessels on the procambium side exhibited lateral water flow toward the procambium. Furthermore, various directions were observed among metaxylem vessels located inside VBs, suggesting that this region of the VB represents a 'middle passage'. These findings suggest that local lateral water flow is regulated according to the relative position of xylem vessels within a VB.

Structural and functional analysis of individual vascular bundles

The number and size of axillary organs depend on the growth conditions and developmental stages, and generally the lowest organs (first branch, B_1 and first cauline leaf, L_1 in **Fig. 2A**) are the largest, as they are in the most advanced developmental stages. Considering that all living tissues are connected to the vasculature of the main stem, we sought to characterize the xylem network by observing changes in the vasculature in serial sections along the height of the stem (**Fig. 2A**). Interestingly, VB organization in the stem is dramatically different before and after the emergence of axillary organs. For example, just before the emergence of B_1 and L_1 (**Fig. 2B**, bottom), a part of a VB (red asterisk) divides from the 'mother bundle' (blue asterisk), resulting in two independent VBs. The distance between these VBs gradually increases as B_1 emerges (**Fig. 2B**; middle). One of these bundles (red asterisk) approaches the branch point, and connects with B_1. Therefore, after B_1 has emerged, only the mother bundle remains in the main stem (**Fig. 2B**,

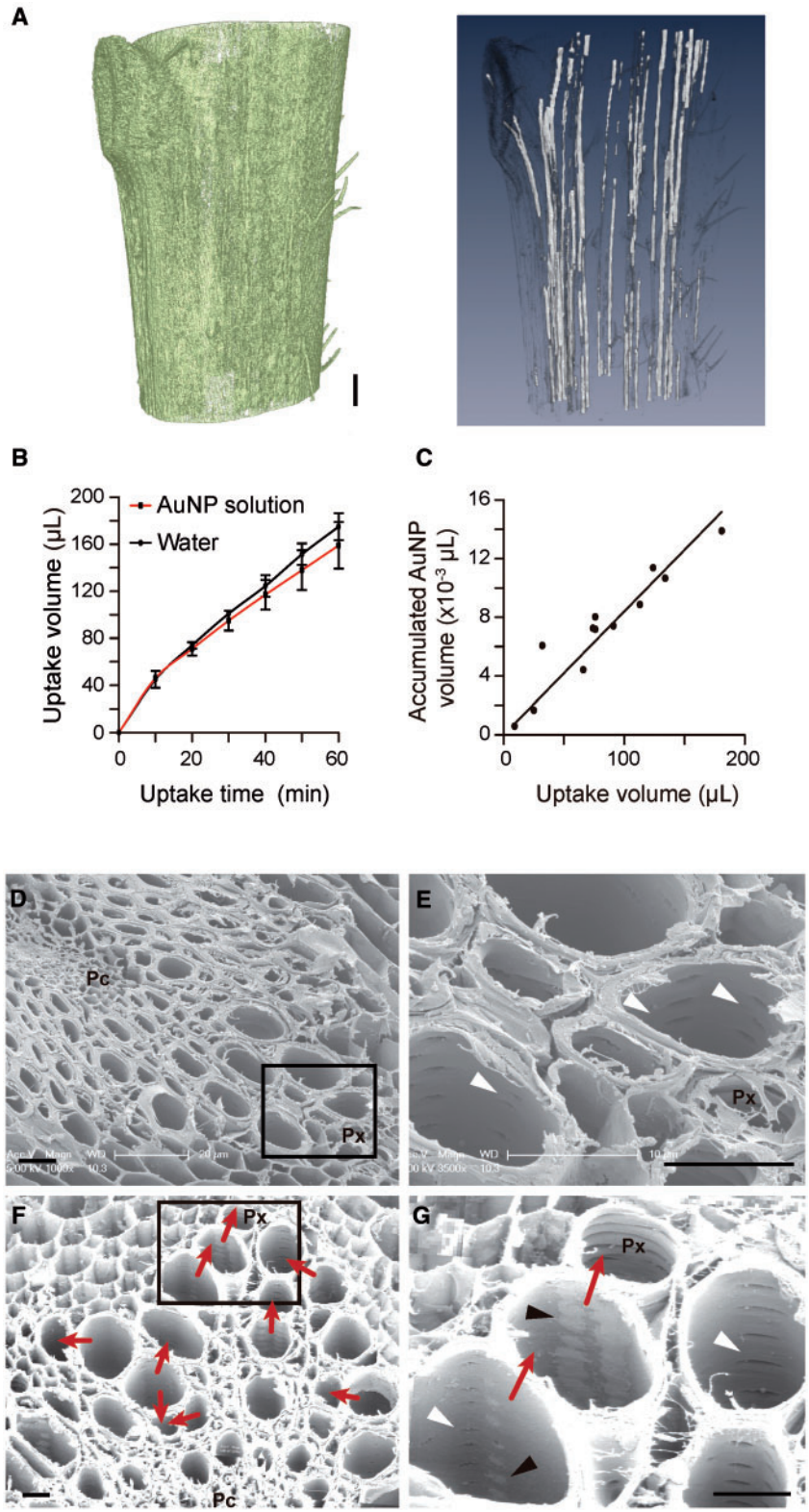

Fig. 1 Visualization of water flow using SXRCT and AuNPs. (A) The 3D rendering of a SXRCT scan of a cut stem base after uptake of AuNP solution. Left, an external view of a stem section. Right, an internal view showing AuNP accumulation in the lumens of individual vessels of a stem. Scale bar = 250 μm. (B) Comparison of the uptake volume of water and that of AuNP solution in cut stems. The uptake volume was measured every 10 min after exposure for 1 h. Error bars, SE ($n = 3$). (C) The uptake volume of AuNP solution was significantly correlated with the accumulated AuNP volume measured by SXRCT ($y = 83917x$; $r^2 = 0.89$; significance, $P < 0.001$). (D–G) SEM images of a stem after 30 min (D and E) and 1 h (F and G) of AuNP solution uptake. The direction of lateral water flow was determined based on the presence or absence of AuNP accumulation at intervessel pits in a 360° observation of the inside surface of cell walls. (E and G) Enlargements of boxed regions of (D) and (F). Arrowheads indicate intervessel pits covered with AuNP (black) or uncovered (white). Px, protoxylem. Pc, procambium. Red arrows, directions of lateral water flow. Scale bars = 10 μm.

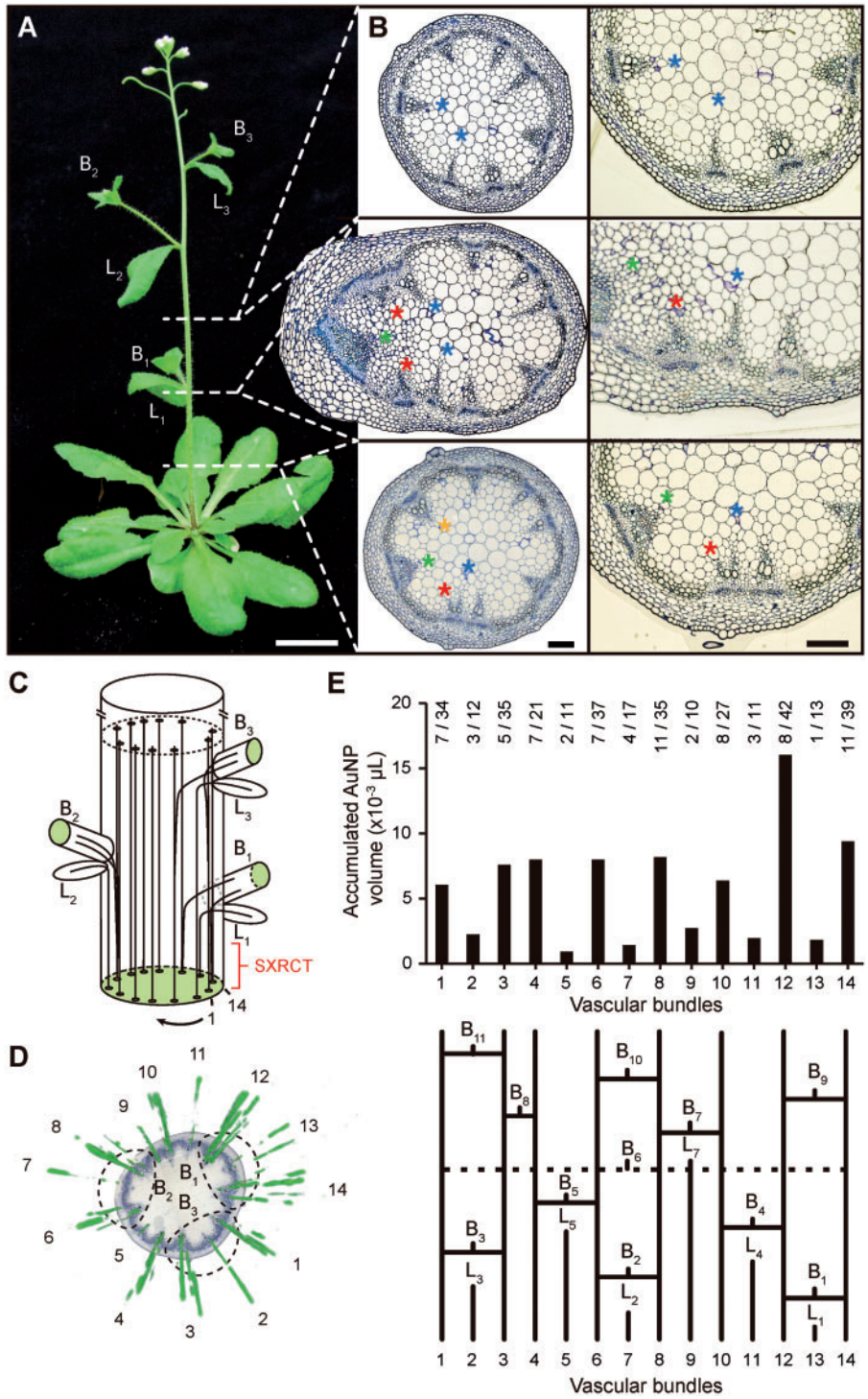

Fig. 2 Histological analysis and water-conducting activity of VBs. (A) An Arabidopsis plant (40 d old; grown under long-day conditions) indicating three different heights at which histological cross-sections were taken. The lowest three branches and three cauline leaves are designated B_1–B_3 and L_1–L_3, respectively, from the base of the stem. (B) Cross-sections showing structural changes in VBs. Before branching (bottom), some vessels (red asterisks) that are connected to a branch are divided from the 'mother' VB (blue asterisks), which remains in the main stem. The yellow asterisk (bottom) indicates a VB not yet dividing, but that begins dividing near the branching point (middle). Green asterisks indicate VBs connected to the cauline leaf. Note that red and green asterisks are not present after branching (top). (C) A schematic diagram of a stem showing the continuity of VBs, which are numbered 1–14 in a clockwise direction at the base. (D) Top view of AuNP-accumulated vessels of the stem in (C) reconstituted by SXRCT after a 30 min uptake of AuNP solution. An image of a histological section of the same stem is merged as the background. Vascular bundles connected to the three branches are indicated with dashed circles. (E) Top, the total volume of accumulated AuNP in individual VBs of the stem. The number of AuNP-accumulated vessels and the total number of vessels in each VB are shown at the top of the chart. Bottom, diagram showing VBs connected to the upper part of the stem with 11 branches. Note that each VB transports a different amount of water to the branches and cauline leaves. Scale bars = 1 cm (A); 100 µm (B).

top). In all cases observed, each branch is connected to two distinct VBs (red asterisks, Fig. 2B; middle) that were derived from VBs in the main stem. Furthermore, these two VBs divide again into several small VBs, which together constitute the vasculature of the branch. Sometimes a VB does not show signs of dividing (yellow asterisk, Fig. 2B, bottom), indicating that two VBs connected to the same branch do not divide from the mother VBs at the same time. L_1 is connected to just one VB (green asterisks in Fig. 2B) located between two VBs that are connected to B_1. As a comparison with general anatomy of seed plants (Esau 1977, Beck 2010), the vessels connected to a branch within a B-type VB correspond to a branch trace, and within an L-type VB to a leaf trace.

Based on the vasculature of a whole stem and the axillary organ number, we speculated that each VB has different water-conducting activity. To test this idea, we reconstructed the vasculature of a cut stem with 11 branches and 14 VBs, and analyzed the vasculature by SXRCT after AuNP solution uptake. Fig. 2C shows the schematic vasculature in the lowest three branches (B_1, B_2 and B_3), the numbering of 14 VBs and the region subjected to SXRCT analysis (Fig. 2D). Only a few xylem vessels in each VB appeared to contain AuNPs (Fig. 2E; numbers, top), indicating that a limited number of vessels are functionally involved in water transport in a given situation. We also confirmed that phloxine B, a hydrophilic fluorescence dye, stained a few vessels within the VB (Supplementary Fig. S4). These results suggest that the water-conducting activities of individual xylem vessels are not identical under given conditions. Furthermore, each VB has distinct water-conducting activities (Fig. 2E, top), which are closely correlated with the number of connected organs (Fig. 2E, bottom). For example, VBs 2, 5, 7, 11 and 13 are connected to fewer tissues than are other VBs. Notably, VB 2 and 13 are connected to only L_1 and L_2, respectively. Also, VBs connected to B_1 (VBs 12 and 14) show relatively high water-conducting activities, as B_1 is in a late developmental stage and has a high water demand. As expected, the total water-conducting activity depends on the water demand of tissues connected to each VB.

Hydraulic architecture: classifying VB types and clustering of xylem vessels within a VB

To characterize the structural and functional features of VBs, we newly defined three distinct types of VBs based on their connection to upper tissues, their shape and xylem vessel organization within them. In addition to a histological analysis, the 3D reconstitution of the vasculature of the dehydrated stem facilitates tracking of the continuity and topological location of successive vessels within each VB (Fig. 3A–C). We distinguished three different types of VBs. (i) The M (main stem)-type VBs are the most common type (Fig. 3C; orange), and consist of vessels arranged in a triangular shape and generally increasing in size towards the pith. (ii) The B (branch)-type VBs are dividing VBs that are connected with a branch, and include not only xylem vessels (Fig. 3C; red) directly connected to a branch but also xylem vessels remaining in the main stem after emergence of branches (blue). (iii) The L (leaf)-type VBs (Fig. 3C; green) are directly connected to the veins of cauline leaves, and consist of one or two rows of protoxylem and metaxylem vessels. The organization of VBs changes dynamically along the height of the stem, particularly near emerging regions of axillary organs such as branches and cauline leaves. Based on our classification, we could reconstitute the changes in VB organization in the stem (Fig. 3D).

We then attempted to define the relationship between the function of xylem vessels and their position within a VB as suggested in Fig. 1F, considering that all vessels are not always active (Fig. 2D, E). To examine whether the position of vessels within each VB is related to the interconnectivity between neighboring conduits, which is crucial for determining the flow path in the xylem network, we visualized intervessel pits using SEM (Fig. 3E–G). Surprisingly, we observed that vessels within a VB are functionally grouped, indicating that the vessels in one subdivision can function as one unit for water transport at a given height. We also found that the configuration of subdivisions is not fixed along the axis of the stem, but rather that the number of xylem vessels belonging to each subdivision and the area of each subdivision are slightly varied depending on the position of boundaries between subdivisions. This flexibility suggests that some vessels on the boundary leave one subdivision and join another, which allows lateral water transfer between subdivisions. To generalize the function of individual vessels within subdivisions in a VB, we classified xylem vessels into three clusters according to their interconnectivity and relative positions in an M- and B-type VB (Fig. 3H–J). Cluster1 consists of large metaxylem vessels facing protoxylem vessels. Cluster2 is localized in the middle of a VB. Cluster3 toward to the procambium consists of the smallest metaxylem vessels. Near the branch where M/B-type transition occurs to form a branch trace, all of the vessels in one side of Cluster2, but only a few vessels in Cluster1 and 3, are connected to the branch. Generally, large xylem vessels are located in Cluster1 and Cluster2. No clusters are distinguishable in L-type VBs, which consist of only a few isolated metaxylem vessels (Fig. 3K).

Regulation of water flow in individual xylem vessels along the height of the plant

To characterize hydraulic regulation along the height of a plant, we analyzed variations in the water transport pathways in conjunction with changes in VB types. The total number of VBs and the level of network ramifications vary with the number of cauline leaves and axillary stems along the height of the plant depending on growth and developmental conditions. Fig. 4A shows the xylem architecture of the lowest three branches (B_1, B_2 and B_3) of a plant with 13 branches. Fourteen independent VBs were classified into eight M-types, four B-types and two L-types at the base of the stem. Each VB was named according to their type and the order of connected organs. For example, the two B-type VBs (B1-1 and B1-2) transport water to B_1. Likewise, L1 is connected to L_1. We compared the number of AuNP-accumulated vessels in each cluster and the water-conducting activity of each cluster at two different heights that exhibited changed VB types. After the cut stem was immersed in AuNP solution for 30 min (at 0 mm), the cut

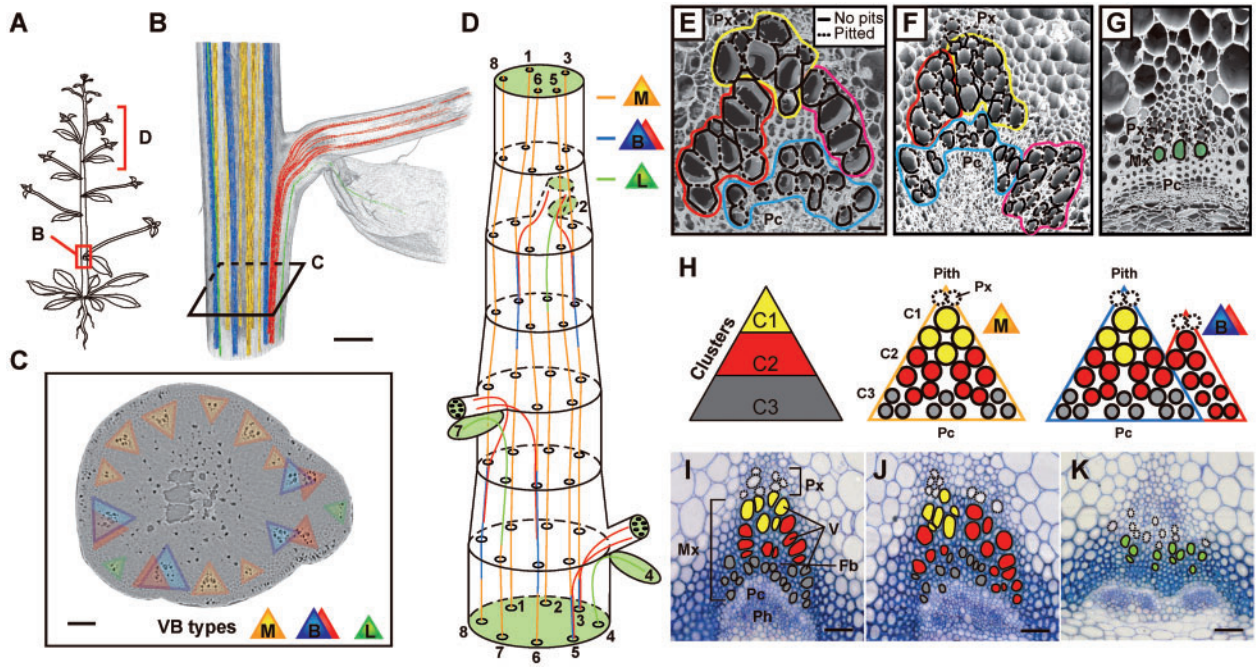

Fig. 3 Classification of VBs based on structural characteristics, and clustering of vessels in a VB. (A) Schematic representation of a dehydrated Arabidopsis plant, indicating the location of the observed segment in (B) and the part illustrated in (D). (B) Side view of the xylem network within the stem reconstructed by SXRCT, including one branch and one cauline leaf. Vessels within the segment are shown in different colors, designating the three different VB types (as in C). (C) Tomographic cross-section below the branch in which VBs are classified into three types, i.e. M-type VBs (orange), B-type VBs (blue and red) and L-type VBs (green). (D) Schematic representation of the change in VB types in the 3D xylem network along the height of the plant. Note the changes in VB types following branching from the base upwards. (E–G) Identification of interconnectivity among xylem vessels of each VB by SEM. Black solid and dashed lines indicate the secondary cell wall of vessels without or with pits, respectively. Colored lines indicate subdivisions that are separated by interconnectivity in an M-type VB (E) and a B-type VB (F). (G) Small isolated vessels in an L-type VB depicted in green. (H) Schematic representations of vessels in three clusters of an M-type VB (center) and a B-type VB (right). Vessels within each cluster are designated as yellow (Cluster1, C1), red (Cluster2, C2) and gray (Cluster3, C3) circles. C1 (yellow) includes vessels close to the protoxylem, C2 (red) includes vessels at both sides of the VB, and C3 (gray) includes vessels beside the procambium. (I–K) Representative histological cross-sections of M-type (I), B-type (J) and L-type (K) VBs. In (I) and (J), the colors of representative vessels in each VB are the same as those in (H). (K) An L-type VB has only a few small vessels, which are not classified into three clusters. Metaxylem vessels are designated as green circles. Px, protoxylem; Mx, metaxylem; V, vessel; Fb, fiber; Pc, procambium; and Ph, phloem. Scale bars = 500 μm (B), 100 μm (C), 20 μm (E–G) and 50 μm (I–K).

stem was re-cut just below B_2 (at 18 mm). The remaining stem was immersed again in AuNP solution for 30 min. The two points were analyzed by SXRCT (**Fig. 4A**). The number of AuNP-accumulated vessels and the total number of vessels in each VB differ at the two points. The two B-type VBs (B1-1 and B1-2; **Fig. 4B**, bottom, at 0 mm) are re-organized into M-type VBs (M9 and M10, top, at 18 mm). At 18 mm, there were up to 58% fewer AuNP-accumulated vessels in each cluster than at 0 mm, especially in Cluster2. In contrast, in the case of the other two B-type VBs (B2-1 and B2-2), the total number of vessels increased from 36 to 40 (B2-1) and from 38 to 51 (B2-2) with proximity to the branch, and the number of AuNP-accumulated vessels increased only in Cluster2. The volume of AuNPs accumulated in Cluster2 is greater at 18 mm than at 0 mm (**Fig. 4C**). Also, in the two M-type VBs (M5 and M7; **Fig. 4B**, bottom) at 0 mm, water is primarily transported through a few vessels located in Cluster1. However, close to B_3, the VBs change to the B-type (B3-1 and B3-2; **Fig. 4B**, top) and the activity and/or number of AuNP-accumulated vessels of Cluster2 increased, especially in B3-1 (**Fig. 4B, C**). Furthermore, other M-type VBs (M1, M3, M6, and M8) seem to change progressively to L-type VBs. Like L-type VBs (L1 and L2), these M-type VBs (finally connected to L_4, L_5, L_3 and L_6, respectively; **Fig. 4D**) had only a few AuNP-accumulated vessels, and there are no significant changes in the number of total vessels and AuNP-accumulated vessels between the two points. These findings indicate that the position and activities of xylem vessels within a VB can change depending on the water demand in each vessel, and that the water-conducting activity of vessels in Cluster2 depends on whether or not a branch is present and also on the distance to the branch, which suggests that water flow to a branch originates from Cluster1.

To confirm this, we sought to identify the pathway that transports water toward a branch (**Fig. 5**). An 80 mm stem section that included three branches (B_1, B_2 and B_3) was removed, and the upper cut end of the stem and the other branches (B_1 and B_3) was sealed to prevent dehydration. The lower cut end was immersed in AuNP solution for 30 min (at 0 mm), while artificial negative pressure (−0.1 MPa) was specifically generated in B_2 via a silicon tube of an appropriate diameter (**Fig. 5A**). Then, the stem was re-cut just below B_2 (at 50 mm) and re-immersed in AuNP solution with the same

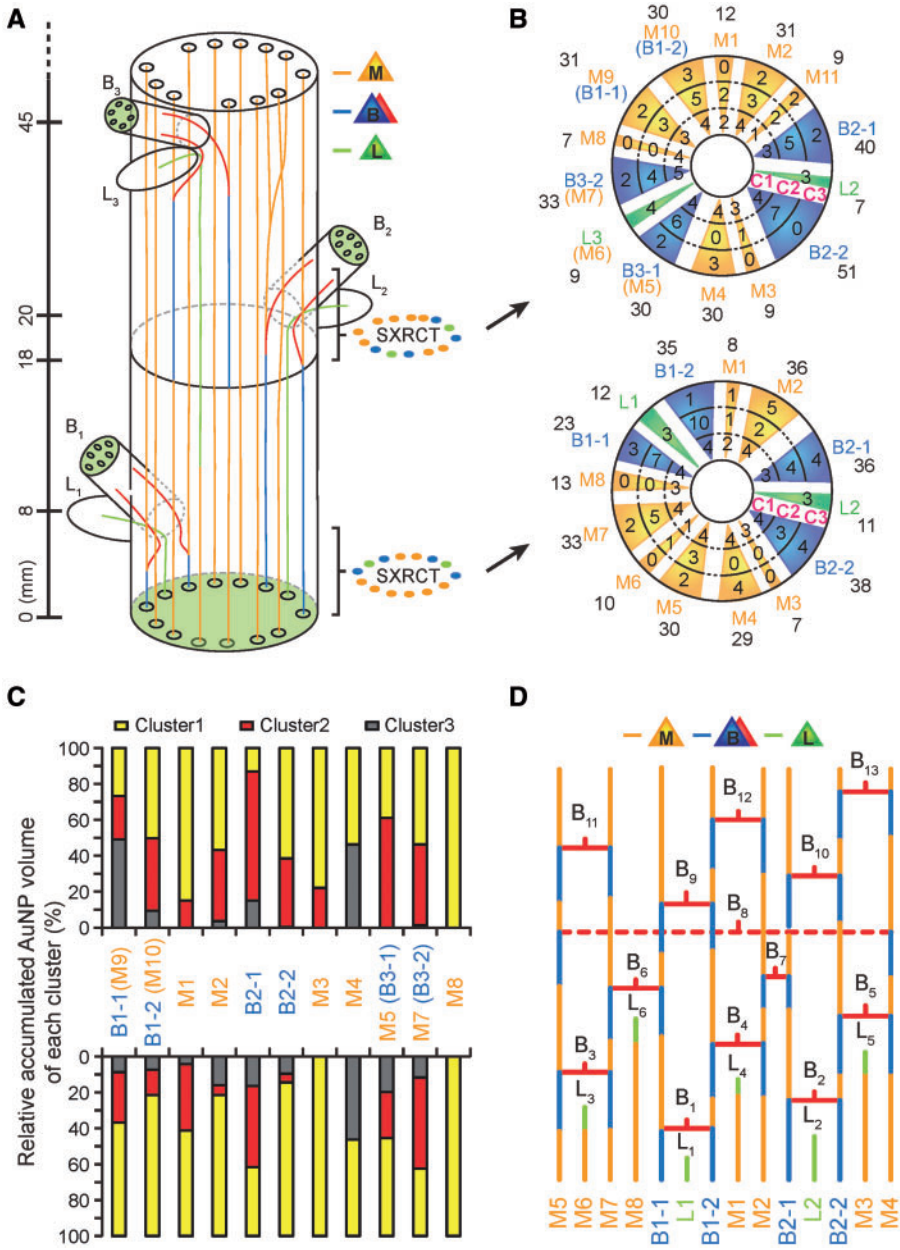

Fig. 4 Changes in water-conducting vessels along the height of the plant. (A) Schematic representation of the stem designating the heights of three branching points (8, 20 and 45 mm) and the two cut ends (0 and 18 mm). The two points analyzed by SXRCT after serial uptake of AuNP solution are shown. Types of VBs analyzed by SXRCT are presented as colored dots on the right. (B) Pie charts indicating the number of AuNP-accumulated vessels in each cluster (inside) and the total vessel number (outside) show the changes in VB types along the height of the plant. (C) The relative volume of AuNP accumulation of each cluster for VBs at the base (0 mm, bottom) and just below B_2 (18 mm, top). (D) A 2D diagram illustrating changes in each VB from the base to the top of the stem. Each VB contributes differently to transporting water to the branches and cauline leaves.

negative pressure generated in the same B_2 for another 30 min. The two points were visualized by SXRCT (**Fig. 5B**), and the distribution of AuNP-accumulated vessels within VBs connected to B_2 (M1 and M3, bottom; B2-1 and B2-2, top) was analyzed (**Fig. 5C**). At 0 mm, AuNP-accumulated vessels were mainly located in Cluster1 in M1 and M3, but at 50 mm, Cluster2 has many AuNP-accumulated vessels in B2-1 and B2-2. In other words, water transported toward B_2 is derived mainly from Cluster1 of M1 and M3, and is transferred laterally to Cluster2 before the VBs are reorganized into B2-1 and B2-2.

Based on the results of the detailed flow analysis in each VB type, we deduced a general water transport pattern that changes along the height of the plant. Most of the water uptake is initiated and propagated through a few large vessels in Cluster1, providing a low resistance pathway for long-distance water transport to the upper tissues. Near a branch, the water flow can diverge into two distinct pathways; axial long-distance water transport still relies on vessels of Cluster1, whereas transport to branches occurs via Cluster2.

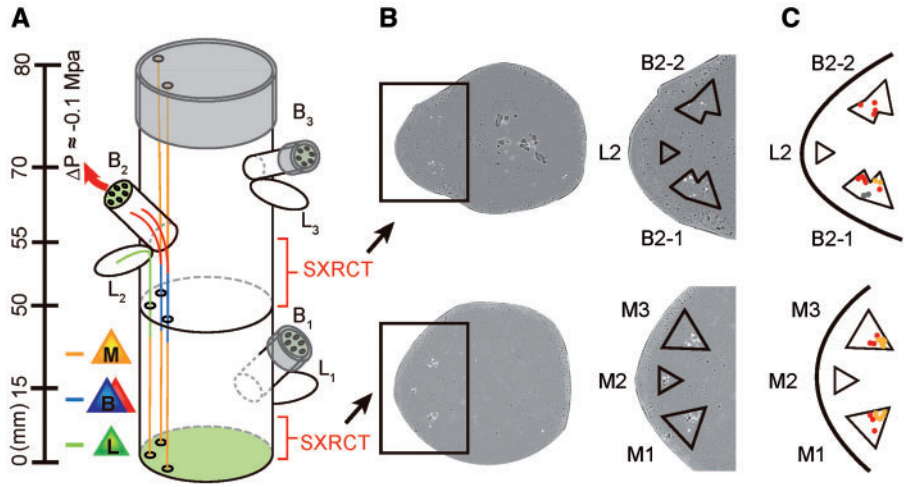

Fig. 5 Pathway of water flow toward a branch. (A) Schematic representation of the experimental set-up used to visualize the water flow pathways driven by artificial negative pressure (arrow) applied to B_2. The heights of three branching points (15, 55 and 70 mm) and the two cut ends (0 and 50 mm). The upper part of the main stem and the two branches B_1 and B_3 were cut and sealed to limit axial flow and to avoid dehydration. The two points analyzed by SXRCT after uptake of AuNP solution are shown. (B) The positions of AuNP-accumulated vessels, which are mainly located in C1 of the two M-type VBs (M1 and M3) at the base (0 mm, bottom), but are located in C2 of the B-type VBs (B2-1 and B2-2) near B_2 (50 mm, top). (C) The locations of AuNP-accumulated vessels in each VB are labeled with colored dots. Cluster1, yellow; Cluster2, red; and Cluster3, gray.

Hydraulic regulation of the xylem network under different water demands

To understand the hydraulic regulation of the xylem network, we examined the effect of different water demands on the functionalities of individual vessels. An intact stem with 10 branches was cut at the base (0 mm) and immersed in AuNP solution. After a 30 min uptake period under natural uptake conditions, the stem was cut at 15 mm (section *N*) above the base. Subsequently, a 10 mm section directly above this point (section *A*) was cut from the remaining stem, and the upper end was attached to a silicon tube to apply artificial negative pressure (−0.1 MPa) although this degree of hydrostatic negative pressure may not occur in Arabidopsis under natural conditions. Then section *A* was allowed to absorb AuNP solution for 30 min. The two sections were analyzed using SXRCT (**Fig. 6A**). Compared with section *N* (bottom), the total number of AuNP-accumulated vessels in section *A* (top) increased by 40% and the total accumulated AuNP volume increased by almost 70% (**Fig. 6B, C**). In addition, an analysis of the activity of each cluster in *M*-type VBs of section *N* confirmed that some vessels of Cluster1 are mainly responsible for long-distance water transport. In contrast, in section *A*, water flux in Cluster2 of *M*-type VBs dramatically increased, to levels similar to those in Cluster1, which indicates that the transpiration-driven negative pressure is preferentially transmitted to the large xylem vessels in Cluster1, but that the vessels in Cluster2 can be additionally activated under environmental and growth conditions that generate a higher water demand if the capacity of vessels in Cluster1 is not sufficient for the given water demand, or the usage of the inactive Cluster2 vessels is more efficient than additional enhancement of Cluster1 activity for the functionality within the xylem network. Furthermore, the activity of each cluster of B-type VBs in section *N* confirmed that Cluster2 of B-type VBs have higher activities than do Cluster2 of *M*-type VBs.

In addition, Cluster3 of *M*-type VBs in section *N* are more active than Cluster2 which consists of larger vessels. Despite the high axial driving force, vessels in Cluster3 of section *A* exhibited lower activities than did those in section *N*. These results suggest that under the given tension, the water-conducting activity of a vessel is not only determined by its size, although size is undoubtedly a major factor. The unexpectedly high activity of vessels of Cluster3 of section *N* suggests that certain factors regulate the hydraulics of the xylem network, including the osmotic pressure from the procambium, xylem–phloem water flow and transpiration from the stem epidermis (Milburn 1996, Tanner and Beevers 2001).

Discussion

A model plant and a novel methodology: usability and cautions

During the early vascular development stage (i.e. primary growth) of most dicot plants, vessel elements and fiber cells originate from the procambium and constitute the xylem of VBs in the stem (Nieminen et al. 2004, Guo et al. 2009). Woody plants have been used to study water flow, and the relatively large size of their stems and vessels (or tracheids) offers technical advantages in various methodologies. Although Arabidopsis inflorescence stems are small and do not show secondary growth under natural growth conditions, the basic components and organogenesis of the vasculature are similar to those of larger plants, and its small size facilitates high-resolution imaging of all individual vessels in a stem, not just a part of the xylem network, which provides a valuable

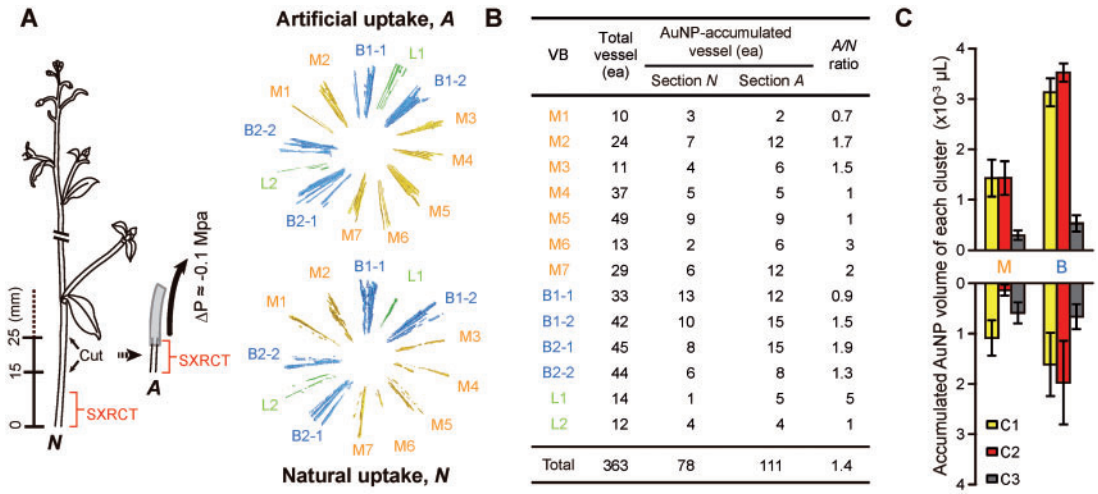

VB	Total vessel (ea)	AuNP-accumulated vessel (ea)		*A/N* ratio
		Section *N*	Section *A*	
M1	10	3	2	0.7
M2	24	7	12	1.7
M3	11	4	6	1.5
M4	37	5	5	1
M5	49	9	9	1
M6	13	2	6	3
M7	29	6	12	2
B1-1	33	13	12	0.9
B1-2	42	10	15	1.5
B2-1	45	8	15	1.9
B2-2	44	6	8	1.3
L1	14	1	5	5
L2	12	4	4	1
Total	363	78	111	1.4

Fig. 6 Hydraulic regulation by water demand. (A) A schematic representation of the experimental set-up used to compare water flow under various uptake demands at the heights of three cut ends (0, 15 and 25 mm). The two points analyzed by SXRCT after serial uptake of AuNP solution are shown. The intensity of the signal of AuNP accumulation increases in section *A* (top) compared with section *N* (bottom). (B) The number of total vessels and AuNP-accumulated vessels in section *N* and *A*. (C) The volume of accumulated AuNP in each cluster in M- and B-type VBs of section *N* (bottom) and section *A* (top). In M-type VBs of section *N*, the water-transporting activity of C1 is dominant, but C2 is also active in B-type VBs. In section *A*, the water-transporting activity of C1 and C2 significantly increases in all VB types. The activity of C3 is higher in section *N* than in section *A*.

hydraulic model to decipher the structure–function relationships of the xylem network (Tixier et al. 2013). Hydrophilic dyes, such as phloxine B, have conventionally been used to visualize water-conducting vessels (Harris 1961, Sano et al. 2005, Umebayashi et al. 2007). However, these dyes rapidly diffuse throughout xylem vessels within small VBs, which limits their ability to reveal the water-conducting activities of individual vessels in Arabidopsis. As an alternative approach, we used AuNPs together with a combination of SXRCT and SEM to visualize the xylem network of the model plant Arabidopsis, and to analyze the water-conducting activity of vessels and track the lateral flow of xylem sap. This methodology enabled us to dissect the functional pathway for water flow and to establish how negative pressure is distributed throughout the xylem network, and would be widely applicable in studies of hydraulic regulation in small samples, such as the small branches of trees, veins of leaves, flowers and fruits. Moreover, this SXRCT tool could provide a new vehicle to explore physiological differences in Arabidopsis plants of different genetic backgrounds, and their various mutants, at different developmental stages and under various growth conditions. Nevertheless, this approach still has several limitations. Firstly, the detection limit of SXRCT, about 1 μm, might not allow the visualization of very low levels of AuNPs in xylem vessels. As such, among the non-water-conducting xylem vessels visualized by SXRCT, few vessels with very weak conducting activities are able to transport water. Secondly, AuNP accumulation on the pit membranes could disturb in vivo water flow. However, under our experimental conditions, we demonstrated that AuNPs physiologically mimic water flow (**Fig. 1B**), and remain proportional to the amount of AuNP solution flow in the vessel lumen (**Fig. 1C**). Although these observations suggest that AuNPs do not block pits and pit membranes within the first 30 min of solution uptake and do not significantly disrupt water flow in Arabidopsis, optimization of experimental conditions to minimize the side effects of AuNP accumulation in other plants with different features in the xylem structures is absolutely necessary. Thirdly, even though cut stems have previously been used to feed dye tracers in studies of xylem hydraulics and sap flow (Booker 1984, Kitin et al. 2010), a shortcoming of this approach is that cutting could disrupt the integrity of the xylem network, abolishing root pressure, and that this effect is ignored. Although cut stems showed similar water uptake properties to intact plants within the first 30 min of exposure to the solution, under our experimental conditions (**Supplementary Fig. S3B**), it is unclear whether any changes occur in the hydraulic properties. Fourthly, the low activities of a few vessels in the artificial flow condition may be partly attributable to vessel length. Vessel length distribution of *A. thaliana* (Tixier et al. 2013) suggests that a 1 cm long segment contained open vessels. If hydraulic resistance of open vessels is extremely low relative to hydraulic resistance of vessels with vessel ends, little water can be conducted through vessels with vessel ends even in the same cluster. Because of these limitations, the SXRCT methodology should be applied cautiously, as in this study.

A proposed model of water flow in the xylem network

Based on the 3D reconstitution of the flow pathways using flow tracers, we established a regulatory model of water flow in the xylem network in the Arabidopsis stem (**Fig. 7**). The key structural and functional unit of this vascular network (i.e. a VB) is composed of multiple xylem vessels of finite length, and lateral flow pathways are enabled by intervessel pits. Our model describes the large plasticity of the xylem network by taking into account the discontinuity of xylem conduits, the variation

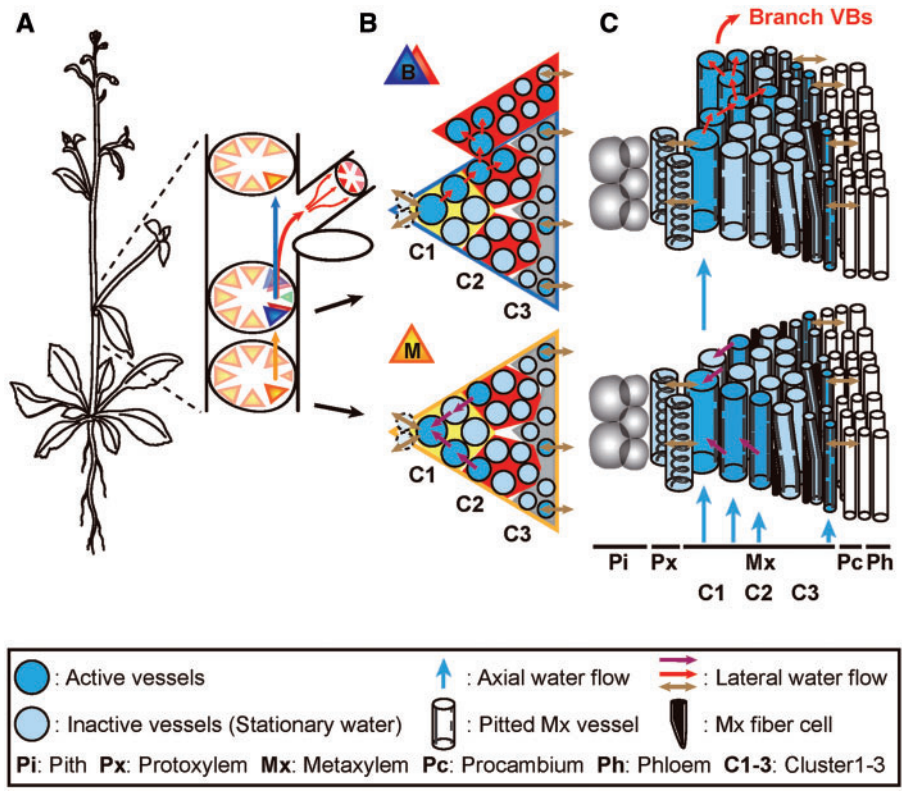

Fig. 7 A model of water flow in the xylem network. (A) A schematic representation of a main stem illustrating water flow and the change in VB types following the emergence of a branch. (B) Cross-sectional organization of M-type (bottom) and B-type (top) VBs. As an example, active (dark blue) and inactive (light blue) vessels are indicated. Purple arrows in an M-type VB indicate lateral flow to C1, which has highly efficient vessels. Red arrows in a B-type VB indicate lateral flow from C1 to C2 (i.e. transport toward a branch). Brown arrows indicate lateral flow to surrounding tissues such as parenchyma in the pith or the procambium and phloem. (C) Three-dimensional organization of M-type (bottom) and B-type (top) VBs. At the base, the axial water flow (blue arrow) for long-distance transport is centralized in large metaxylem vessels of C1. Near a branch, metaxylem vessels of C2 in B-type VBs are subjected to the negative pressure from a branch, and thus local lateral flow (red arrows) from C1 to C2 occurs.

in vessel number and size at different positions within the functional unit, and the interconnectivity between xylem vessels. In our model, water transport is achieved by a limited number of large xylem vessels with a low hydraulic resistance for long-distance water transport (i.e. the structural features of vessels in Cluster1). At a certain height, water is distributed towards the source of water demand, such as the pith, procambium or axillary organs. The direction of lateral water flow through intervessel pits is determined by local differences in water potential among adjacent vessels. Each cluster (Cluster1, 2 and 3) at distinct positions within a VB naturally mediates water distribution to the pith, procambium and phloem. During branching, one side of Cluster2 is mainly connected to a branch, so that water in Cluster1 is transferred to Cluster2 via a lateral flow pathway before being reorganized entirely into B-type VBs. These general principles of efficient water transport and distribution can be applied to any scale of the stem. In the branch vasculature, the number of xylem vessels and VBs are reduced in accordance with the small diameter of the branch, but the structural and functional organization remains similar to that of the main stem. Only a limited number of actively water-conducting vessels ensure hydraulic efficiency, and water distribution to surrounding tissues is executed by xylem vessels in each position of a VB. On the other hand, to enhance hydraulic safety, the water supply to a branch could be ensured by two distinct B-type VBs of the main stem, such that one B-type VB can complement the functionality of the other B-type VB. Also, the high degree of interconnection among xylem vessels increases the risk of an embolism spreading to other vessels via intervessel pits when cavitation occurs (Hacke et al. 2006, Loepfe et al. 2007); however, the segmentation of vessels into subdivisions prevents this risk to some extent. Vessels that do not conduct water, or conduct water very slowly, might function as a transient water storage compartment, ensuring safe water management, as do fibers, parenchyma cells and procambium (Tyree and Ewers 1991), to increase tolerance to water stress, such as drought.

Overall, this study shows that water transport pathways and the water-conducting activities of vessels of Arabidopsis are regulated structurally by altering the spatial arrangement of individual vessels within the 3D network, and physiologically by responding to the plant's water demand and capacitance. The structure–function relationships of the xylem network revealed in this study provide the key elements for designing or screening ideotypes with a hydraulic architecture that is adapted to specific environmental conditions.

Materials and Methods

Plant materials and growth conditions

All plants used in this study were *A. thaliana* (Col-0) grown in controlled environmental chambers (23°C, 50–70% humidity and approximately 70 μmol m^{-2} s^{-1} cool fluorescent light). Unless stated otherwise, after 4 weeks of growth under short-day conditions (10 h light, 14 h dark), plants were transferred to long-day conditions (16 h light, 8 h dark) to induce bolting of the inflorescence stems. Except for the water uptake experiment, which evaluated plants at different growth stages, all experiments were carried out using the cut stems (>30 cm) of plants over 17 DAB, and the height and weight of plants and the number of branches and cauline leaves were determined prior to each experiment to select phenotypically similar plants.

Design and fabrication of hydrophilic gold nanoparticles (AuNPs)

Hydrophilic AuNPs of approximately 20 nm in diameter were used as flow tracers to visualize sap transport, and the concentration of AuNP solution was 2.4×10^{10} AuNPs μl^{-1} (Ahn et al. 2010, Ahn et al. 2013).

Solution uptake experiments

Intact plants or stems cut under water to prevent embolisms from forming were immersed in a vial containing either water or AuNP solution. The uptake volume of the solution was determined based on the volume measurement of solution remaining in the vials at 10 min intervals. All uptake experiments were carried out in the chamber in which plants were grown. Artificial negative pressure was applied using a syringe pump. The upper cut end of stem sections or branches was connected to the syringe via a silicon tube and the negative pressure was monitored using a cell pressure probe. The pressure value, i.e. the gauge pressure, was maintained at approximately −0.1 MPa throughout the experiments.

Synchrotron X-ray computed tomography (SXRCT)

SXRCT was mainly conducted at the X-ray Micro Imaging beamline 6D of the Pohang Light Source-II (Pohang Accelerator Laboratory, Pohang, Korea). The X-ray intensity irradiated was approximately 2.8×10^{-2} W mm^{-2}. The distance between the 3D sample stage and the $CdWO_4$ scintillator crystal was set between 30 and 50 cm to obtain images with sufficient phase contrast effects (Kim and Lee 2010). The stem section (1–2 cm) was cut, immediately frozen in liquid nitrogen and placed on the tomography stage with a cryojet system to prevent thawing. The length visualized using SXRCT is 7.2 mm in each section. The stage was rotated from 0 to 180° in increments of 0.5°, yielding 360 two-dimensional projections per sample (exposure time, 10 ms). Each projection was visualized at a ×5 or ×10 magnification and images were captured with a CCD camera (4,008 × 2,672 pixels, VM-11M, Vieworks), giving a field of view (FOV) of approximately 7.2×4.8 or 3.6×2.4 mm^2, respectively. The best spatial resolution was about 1 μm. Complementary natural and artificial uptake experiments were performed at beamline BL13W1 of the Shanghai Synchrotron Radiation Facility (SSRF, Shanghai, China). Two-dimensional X-ray images were reconstructed into cross-sectional images with Octopus software (inCT, Belgium). These image sequences were stacked to reconstitute 3D images using Amira software (FEI Visualization Sciences Group). Each xylem vessel in a cross-sectional slice of the reconstituted tomography was segmented, and the volume of AuNPs accumulated in xylem vessels was quantitatively evaluated using the volume-rendering tool of Amira software.

Histological and SEM analysis

For histological analysis, stem segments of at least 5 mm in length were cut with a razor blade and placed in glass vials containing 3% (v/v) glutaraldehyde. The vials were degassed under vacuum (250 mbar) for 15 min and kept at 4°C for at least 3 h. Samples were dehydrated in a series of graded acetone [30–90% and 3 × 100% (v/v) for at least 15 min for each step] and embedded in low-viscosity (Spurr's) resin (Electron Microscopy Sciences). Thin sections (2 μm) were cut with a rotary microtome (RM2265, Leica), stained in aqueous 0.01% (w/v) toluidine blue O (Sigma) for 1 min and imaged using a light microscope (Axioplan 2, Carl Zeiss).

Samples for SEM were cut in 1–2 mm sections with a razor blade, fixed in 3% (v/v) glutaraldehyde, dehydrated in a graded series of ethanol, replaced with isoamyl acetate [25, 50, 75% and 3 × 100% (v/v) for 15 min for each step], dried with a CO_2 critical point drying system (HCP-2, Hitachi) and coated with gold using an ion coater (PS-1200, PARAONE). The specimen was examined using a field-emission scanning electron microscope (XL30S FEG FE-SEM, Phillips) with a secondary electron detector. The SEM stage was tilted and rotated so that pits inside the cell wall of metaxylem vessels could be observed and analyzed.

Statistical analysis

Quantitative data were subjected to two-tailed Student's *t*-tests using SPSS software.

Supplementary data

Supplementary data are available at PCP online.

Funding

This work was supported by the National Research Foundation of Korea (NRF) grant funded by the Korean government (MSIP) [Creative Research Initiatives (Diagnosis of Biofluid Flow Phenomena and Biomimic Research) (No. 2008-0061991) to S.J.L.]; the Ministry of Science, ICT and Future Planning (MSIP) [Advanced Biomass R&D Center (ABC-2010-0029720) to I.H.]; Ministry of Agriculture, Food and Rural Affairs (MAFRA) [iPET (Korea Institute of Planning and Evaluation for Technology in Food, Agriculture, Forestry and Fisheries) (309017-5) to I.H.].

Acknowledgments

We are grateful to the Pohang Accelerator Laboratory (Pohang, Korea) and the Shanghai Synchrotron Radiation Facility (Shanghai, China).

Disclosures

The authors have no conflicts of interest to declare.

References

Ahn, S., Jung, S.Y. and Lee, S.J. (2013) Gold nanoparticle contrast agents in advanced X-ray imaging technologies. *Molecules* 18: 5858–5890.

Ahn, S., Jung, S.Y., Lee, J.P., Kim, H.K. and Lee, S.J. (2010) Gold nanoparticle flow sensors designed for dynamic X-ray imaging in biofluids. *ACS Nano* 4: 3753–3762.

Beck, C.B (2010) *In* An Introduction to Plant Structure and Development: Plant Anatomy for the Twenty-First Century, 2nd edn pp. 123–169. Cambridge University Press, Cambridge.

Booker, R.E. (1984) Dye-flow apparatus to measure the variation in axial xylem permeability over a stem cross-section. *Plant Cell Environ.* 7: 623–628.

Brodersen, C.R., McElrone, A.J., Choat, B., Matthews, M.A. and Shackel, K.A. (2010) The dynamics of embolism repair in xylem: in vivo visualizations using high-resolution computed tomography. *Plant Physiol.* 154: 1088–1095.

Brodersen, C.R., Roark, L.C. and Pittermann, J. (2012) The physiological implications of primary xylem organization in two ferns. *Plant Cell Environ.* 35: 1898–1911.

Dixon, H.H. and Joly, J. (1894) On the ascent of sap. *Ann. Bot.* 8: 468–470.

Esau, K (1977) *In* Anatomy of Seed Plants, 2nd edn pp. 257–294. Wiley, New York.

Guo, Y., Qin, G.J., Gu, H.Y. and Qu, L.J. (2009) Dof5.6/HCA2, a dof transcription factor gene, regulates interfascicular cambium formation and vascular tissue development in Arabidopsis. *Plant Cell* 21: 3518–3534.

Hacke, U.G., Sperry, J.S., Wheeler, J.K. and Castro, L. (2006) Scaling of angiosperm xylem structure with safety and efficiency. *Tree Physiol.* 26: 689–701.

Harris, J.M. (1961) Water-conduction in the stems of certain conifers. *Nature* 189: 678–679.

Holbrook, N.M., Ahrens, E.T., Burns, M.J. and Zwieniecki, M.A. (2001) In vivo observation of cavitation and embolism repair using magnetic resonance imaging. *Plant Physiol.* 126: 27–31.

Holbrook, N.M. and Zwieniecki, M.A. (2005) *In* Vascular Transport in Plants Elsevier Academic Press, Amsterdam.

Johnson, B. and Dixon, J.R. (1965) Ascent of sap in trees—effect of negative absolute pressure on flow resistance. *Nature* 208: 1347.

Kim, H.K. and Lee, S.J. (2010) Synchrotron X-ray imaging for nondestructive monitoring of sap flow dynamics through xylem vessel elements in rice leaves. *New Phytol.* 188: 1085–1098.

Kim, H.K., Park, J. and Hwang, I. (2014) Investigating water transport through the xylem network in vascular plants. *J. Exp. Bot.* 65: 1895–1904.

Kitin, P., Voelker, S.L., Meinzer, F.C., Beeckman, H., Strauss, S.H. and Lachenbruch, B. (2010) Tyloses and phenolic deposits in xylem vessels impede water transport in low-lignin transgenic poplars: a study by cryo-fluorescence microscopy. *Plant Physiol.* 154: 887–898.

Lee, J., Holbrook, N.M. and Zwieniecki, M.A. (2012) Ion induced changes in the structure of bordered pit membranes. *Front. Plant Sci.* 3: 55.

Loepfe, L., Martinez-Vilalta, J., Pinol, J. and Mencuccini, M. (2007) The relevance of xylem network structure for plant hydraulic efficiency and safety. *J. Theor. Biol.* 247: 788–803.

Milburn, J.A. (1996) Sap ascent in vascular plants: challengers to the cohesion theory ignore the significance of immature xylem and the recycling of Munch water. *Ann. Bot.* 78: 399–407.

Nieminen, K.M., Kauppinen, L. and Helariutta, Y. (2004) A weed for wood? Arabidopsis as a genetic model for xylem development. *Plant Physiol.* 135: 653–659.

Ryu, J., Ahn, S., Kim, S.-G., Kim, T. and Lee, S.J. (2014) Interactive ion-mediated sap flow regulation in olive and laurel stems: physicochemical characteristics of water transport via the pit structure. *PLoS One* 9: e98484.

Sano, Y., Okamura, Y. and Utsumi, Y. (2005) Visualizing water-conduction pathways of living trees: selection of dyes and tissue preparation methods. *Tree Physiol.* 25: 269–275.

Santiago, M., Pagay, V. and Stroock, A.D. (2013) Impact of electroviscosity on the hydraulic conductance of the bordered pit membrane: a theoretical investigation. *Plant Physiol.* 163: 999–1011.

Scheenen, T.W.J., Vergeldt, F.J., Heemskerk, A.M. and Van As, H. (2007) Intact plant magnetic resonance imaging to study dynamics in long-distance sap flow and flow-conducting surface area. *Plant Physiol.* 144: 1157–1165.

Tanner, W. and Beevers, H. (2001) Transpiration, a prerequisite for long-distance transport of minerals in plants? *Proc. Natl Acad. Sci. USA* 98: 9443–9447.

Tixier, A., Cochard, H., Badel, E., Dusotoit-Coucaud, A., Jansen, S. and Herbette, S. (2013) Arabidopsis thaliana as a model species for xylem hydraulics: does size matter?. *J. Exp. Bot.* 64: 2295–2305.

Tyree, M.T. (1997) The cohesion–tension theory of sap ascent: current controversies. *J. Exp. Bot.* 48: 1753–1765.

Tyree, M.T. and Ewers, F.W. (1991) The hydraulic architecture of trees and other woody plants. *New Phytol.* 119: 345–360.

Tyree, M.T. and Zimmermann, M.H. (2002) *In* Xylem Structure and the Ascent of Sap Springer-Verlag, Berlin.

Umebayashi, T., Utsumi, Y., Koga, S., Inoue, S., Shiiba, Y., Arakawa, K. et al. (2007) Optimal conditions for visualizing water-conducting pathways in a living tree by the dye injection method. *Tree Physiol.* 27: 993–999.

Van As, H. (2007) Intact plant MRI for the study of cell water relations, membrane permeability, cell-to-cell and long distance water transport. *J. Exp. Bot.* 58: 743–756.

Wei, C., Steudle, E. and Tyree, M.T. (1999) Water ascent in plants: do ongoing controversies have a sound basis?. *Trends Plant Sci* 4: 372–375.

Wheeler, J.K., Huggett, B.A., Tofte, A.N., Rockwell, F.E. and Holbrook, N.M. (2013) Cutting xylem under tension or supersaturated with gas can generate PLC and the appearance of rapid recovery from embolism. *Plant Cell Environ.* 36: 1938–1949.

Wheeler, T.D. and Stroock, A.D. (2008) The transpiration of water at negative pressures in a synthetic tree. *Nature* 455: 208–212.

Wistuba, N., Reich, R., Wagner, H.J., Zhu, J., Schneider, H., Bentrup, F.W. et al. (2000) Xylem flow and its driving forces in a tropical liana: concomitant flow-sensitive NMR imaging and pressure probe measurements. *Plant Biol.* 2: 579–582.

Zwieniecki, M.A., Melcher, P.J. and Michele Holbrook, N. (2001) Hydrogel control of xylem hydraulic resistance in plants. *Science* 291: 1059–1062.

Zwieniecki, M.A., Orians, C.M., Melcher, P.J. and Holbrook, N.M. (2003) Ionic control of the lateral exchange of water between vascular bundles in tomato. *J. Exp. Bot.* 54: 1399–1405.